NDT&E International 67 (2014) 31–35

Contents lists available at ScienceDirect

NDT&E International

journal homepage: www.elsevier.com/locate/ndteint

Quantification of the phase fraction in steel using an electromagnetic sensor

L. Zhou [a,*], J. Liu [a], X.J. Hao [a], M. Strangwood [a], A.J. Peyton [b], C.L. Davis [a]

[a] School of Metallurgy of Materials, University of Birmingham, Edgbaston, Birmingham, UK
[b] School of Electrical and Electronic Engineering, University of Manchester, Manchester, UK

ARTICLE INFO

Article history:
Received 4 January 2014
Received in revised form
23 June 2014
Accepted 27 June 2014
Available online 11 July 2014

Keywords:
Relative permeability
Magnetic sensors
Dual phase steels
Ferromagnetic materials
Finite element analysis

ABSTRACT

The effect of ferrite fraction, in 0.17–0.8 wt% C steels with ferrite–pearlite microstructures, on multi-frequency electromagnetic (EM) sensor readings has been studied. The measured initial relative permeability values agreed well with finite element microstructure model predictions. The EM sensor low frequency inductance value is sensitive to changes in relative permeability and the sensor can measure ferrite fraction in dual-phase steels. Therefore, EM sensors could be used to assess dual-phase (ferrite + pearlite/bainite/martensite) steel microstructures in a non-contact, non-destructive manner.

1. Introduction

Strip steels with dual or multi-phase structures are widely used in the automotive industry. The microstructure of dual phase steels often consists of a matrix of ferrite, with typically 20% dispersion of second phase (e.g. martensite or bainite) islands [1]. The microstructure is produced either by controlling the transformation of austenite after hot rolling or by intercritical annealing after cold rolling [2]. The amount and type of any second phase play an important role in determining mechanical properties. In order to obtain accurate quality control, it is important to be able to monitor the phase fraction non-destructively. Several techniques could be employed such as X-ray, electromagnetic or ultrasonic sensors [3–6]; among which, electromagnetic (EM) techniques have attracted much attention due to their advantages of being non-contact, having a short response time and being relatively inexpensive.

EM sensors exploit the difference in magnetic properties, such as relative permeability, and electrical conductivity between samples with different microstructural phase balances. In ferromagnetic steels, the change in relative permeability has a significant effect. Previously, multi-frequency EM sensors have been shown to be able to measure austenite/ferrite fraction from 0% to 100% in model (HIPped austenitic/ferritc stainless steel powder) alloys [7,8]. The large difference in magnetic properties of ferrite (ferromagnetic) and austenite (paramagnetic) phases makes the change in signal large and hence relatively easy to measure. EM sensors have also measured the levels of decarburisation (variation in ferrite content with depth) in steel rod [9,10]. The approach adopted to relate the overall steel EM sensor signal to its microstructure has been to construct a finite element (FE) model for the microstructure (phase, region size and distribution). The EM properties of the individual phases are assigned to those regions to give the overall EM properties of the steel. Within the model the particular sensor geometry is included (e.g. two-dimensional axisymmetric for a cylindrical sample and tubular sensor [10]) and the interaction with the steel and any external circuits predicted. In this way different microstructures and sensor designs can be compared.

When considering the effective electrical or magnetic property of a material which has two components with contrasting properties, power law models have been popularly used [8,11–13]. The power law model predicts the effective permeability as

$$\mu_e^\beta = (1-f)\mu_1^\beta + f\mu_2^\beta \quad (1)$$

where μ_1 and μ_2 are the relative permeability values of the first and second phase respectively, f is the fraction of the second phase, and β is a dimensionless parameter. Examples of the power law are the Birchak formula ($\beta=1/2$) [13] and the Looyenga formula ($\beta=1/3$) [12] for prediction of the dielectric constant of mixtures. Hao et al. developed a FE microstructure model to predict the relative permeability based on actual microstructures. The model was found to give good agreement with measured

* Corresponding author. Tel.: +44 121 4145174; fax: +44 121 4147468.
E-mail address: l.zhou@bham.ac.uk (L. Zhou).

http://dx.doi.org/10.1016/j.ndteint.2014.06.007
0963-8695/

results over the whole range of ferrite fraction for austenite/ferrite microstructures. However, the power-law model with $\beta=1/2$ did not give a good fit, whilst $\beta=1/3$ only gave good agreement with measured results at ferrite fractions above 40% (samples with ferrite fractions below 40% would require a much smaller β value to give good fitting) [8]. Large changes in EM signal have been reported for ferrite–austenite microstructures as austenite is paramagnetic and ferrite is ferromagnetic, however, the majority of multi-phase steel microstructures contain a mix of ferromagnetic phases (i.e. ferrite, pearlite, bainite and martensite). Whilst EM sensors have been employed on-line for measuring phase balance during transformation after steel hot rolling, i.e. microstructures of ferrite and austenite [14], research is needed to determine if an EM sensor can quantify the phase balance in steel microstructures comprised of different ferromagnetic phases. In this paper, the initial relative permeability values of ferrite/pearlite microstructures with different ferrite fractions were determined by a fitting the EM sensor readings with the FEM model. The results have been compared to power law models and FEM microstructure modelling results.

2. Materials and methods

Melting grade (pure) iron and hot rolled C–Mn steels with different carbon contents have been tested with an EM sensor. The chemical compositions of the steels used are given in Table 1.

Metallographic samples were taken in the transverse direction of the steels, polished to an OPS finish and etched in 2% nital. The samples were imaged using a Zeiss Akioskop-2 optical microscope equipped with Axiovision 4.6.3 image capture software. The ferrite fraction and ferrite grain size of the samples were analysed using "Image J" image analysis software. The hardness was measured on polished samples by Vickers micro-hardness measurement with a 500 g load.

Samples for laboratory EM measurements (cylindrical shape with 4.95 mm diameter and 50 mm length) were machined from the as-received steel. The EM sensor, which is similar to that used in [10], has exciting and sensing coils that are air-cored. Each coil has an inner diameter of 7.95 mm, 0.2 mm height, 10.5 mm length and 56 turns. The coils were driven by a frequency response analyser (SL1250) from 10 Hz to 65,000 Hz, and the real inductance values were determined from mutual inductance measurements. It should be mentioned that the lab based axial sensor with machined cylindrical samples was used in this study for the relative permeability modelling. The principle of the sensor is the same to a detector type (H shape/U shape) EM sensor, which can be applied for industrial use. Electrical resistivity measurements were performed at room temperature using a conventional four point DC method with a Cropico DO5000 microohmmeter. Each resistivity value was determined by taking the average of 10 measurements on the same sample used for EM sensor measurements. The experimental measured EM sensor output together with the resistivity value were used with a two-dimensional COMSOL FE model developed for the sensor-sample geometry, and the relative permeability was predicted by fitting the modelled results to the experimentally measured ones. The geometry

Table 1
Chemical composition for the steel samples used in this work, all in wt%.

	C	Si	Mn	S	P	Cu
0.17C	0.17	0.28	0.80	0.03	0.01	0.09
0.38C	0.38	0.26	0.75	0.03	0.02	0.12
0.53C	0.53	0.29	0.72	0.01	0.02	0.09
0.80C	0.80	0.20	0.96	0.03	0.02	0.02

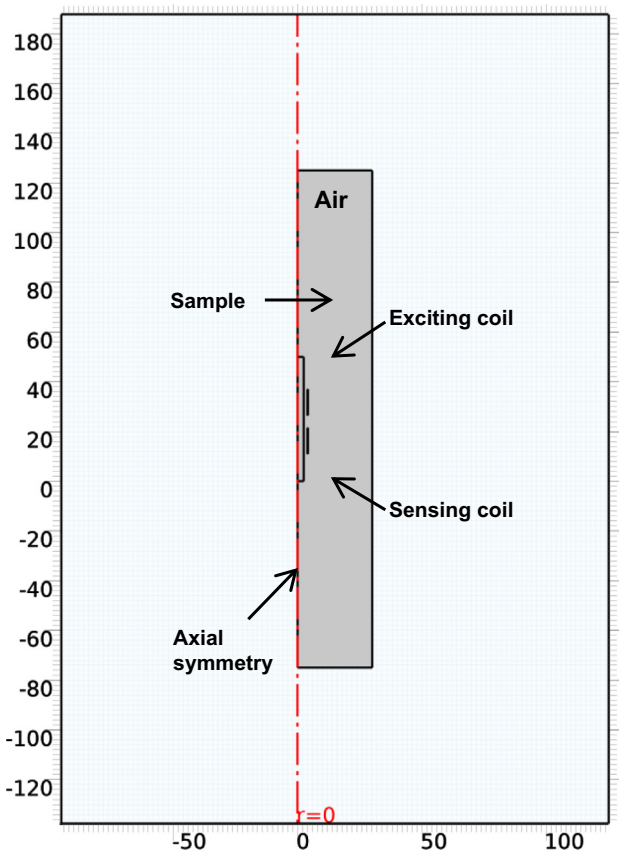

Fig. 1. Geometry setup of the sensor and sample in the FE sensor output model.

setup of the sensor and sample in the model is shown in Fig. 1. The exterior boundaries were set as magnetic insulation and the interior boundaries were set as continuity. Extra fine physics controlled mesh (defined by COMSOL software) was applied to the entire geometry with refined mesh to the sample geometry. The complete mesh of the model consists of 14,782 domain elements and 758 boundary elements. Computation time for each fitting is about 15 min using a quad core (i7) processor with 16G RAM. The details of the fitting method is described in [15].

3. Results and discussion

Optical microstructures of the pure iron, 0.17C, 0.38C, 0.53C and 0.8C as-received samples using a 40× objective are shown in Fig. 2. Table 2 shows a summary of the average ferrite grain size (ECD), ferrite percentage, hardness and resistivity with standard deviation values. The resistivity value increases with carbon content due to the different amounts of pearlite formed.

The measured real inductance versus frequency (logarithmic scale) results for the as-received pure iron, 0.16C, 0.53C and 0.8C steel samples, using the EM sensor are shown in Fig. 3. The EM field produced by the exciting coil in the sensor acts on the steel samples in two ways [10]. At lower frequencies, it tends to magnetise the sample thus an inductance value occurs. Here, the relative permeability of the sample dominates the inductance value. Secondly, the change in magnetic field induces eddy currents that oppose the driving current and the inductance decreases. As the frequency increases, eddy currents become more important so that the real inductance begins to decrease and eventually the EM signal approaches a very low inductance value, where the samples cannot be easily distinguished. The low frequencies (below approximately 100 Hz) real inductance values

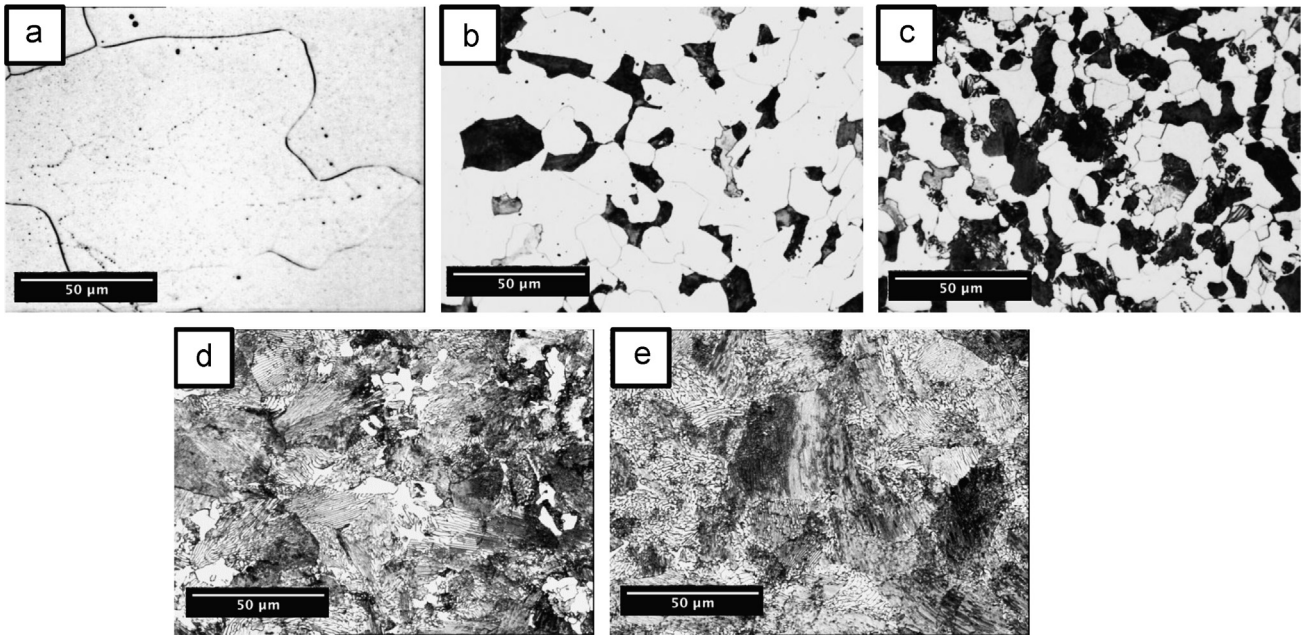

Fig. 2. Optical microstructures of (a) pure iron, (b) 0.17C, (c) 0.38C, (d) 0.53C and (e) 0.8C as-received samples at ×400 magnification.

Table 2
Summary of the microstructure, hardness and resistivity values of the ferrite–pearlite microstructures.

Sample	Average ferrite grain size (μm)	Ferrite%	Hardness (HV)	Resistivity (nΩ m)
Pure iron	155 ± 68.1	100	72.8 ± 1.1	104.0 ± 0.3
0.17C	24.5 ± 10.7	70.8 ± 1.8	146.8 ± 0.4	210.9 ± 0.1
0.38C	14.0 ± 5.8	48.9 ± 1.2	171.3 ± 1.3	218.6 ± 0.2
0.53C	8.0 ± 3.7	9.0 ± 0.7	224.7 ± 2.1	230.1 ± 0.2
0.8C	–	0	277.2 ± 3.2	243.7 ± 0.3

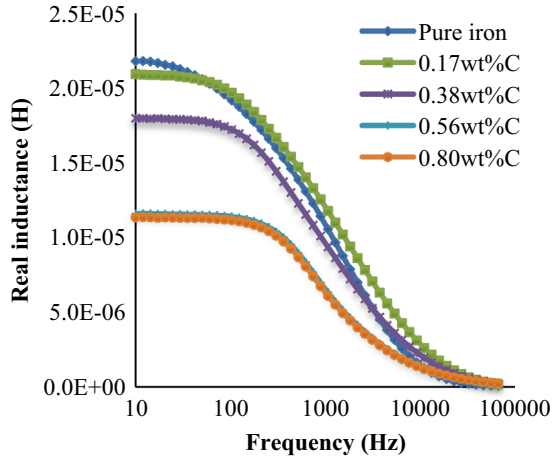

Fig. 3. Real inductance changes with frequency for pure iron, 0.17C, 0.38C, 0.53C and 0.8C as-received (i.e. ferrite + pearlite) steel samples.

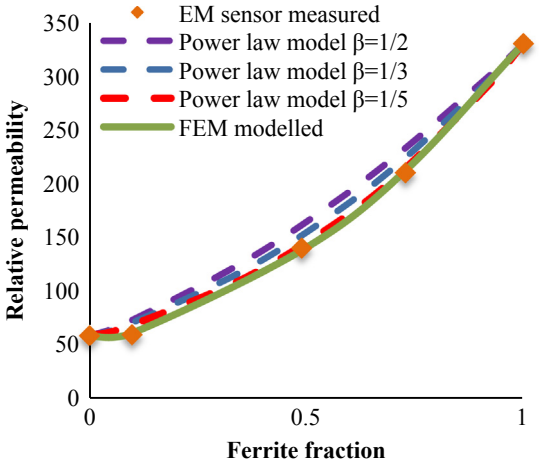

Fig. 4. Relative permeability change with ferrite fraction, FEM modelled results were compared with the power-law model and the experimental fitted results.

decrease with the increase in carbon content up to 0.53 wt% C; this is due to the increasing fraction of pearlite present in the steel, which is known to have a much lower relative permeability value than ferrite [10,16]. It can be seen that the 0.53C and 0.8C steels show little difference in real inductance value at low frequency despite the former sample containing 9% ferrite whilst the latter contains no ferrite. The reason for this is discussed below. It can be seen in Fig. 3 that the pure iron sample shows a slightly different real inductance–frequency curve shape (the inductance starts to decrease earlier); this is due to the higher relative permeability and much lower resistivity (stronger eddy current effect) of the pure iron sample compared to the C–Mn samples.

The relative permeability values calculated from the FE model are plotted against the ferrite fraction in the different steel microstructures as experimental data points in Fig. 4. It can be

seen that there is an increase in the relative permeability value as the ferrite fraction increases. The small difference in relative permeability between the 0.53C and 0.8C steels is believed to be due to the ferrite regions in the 0.53C steel being unconnected (shown in Fig. 2d) and hence not contributing much to the effective permeability of the sample. This is similar to the effect reported by Yin et al. who found that in austenite+ferrite steel samples a low fraction of ferrite ($<40\%$), present as isolated regions due to the powder processing fabrication route, did not result in much increase in permeability for both the measured and FE modelled results [7]. The relative permeability values, determined by fitting the experimental EM sensor results with the FE model, for single-phase pearlite and ferrite are 58.6 and 330 respectively. The value for pearlite agrees well (within 6%) with Thompson et al. [16], who reported that the initial relative permeability of fully pearlitic phase (in a 0.87 wt% C steel) is 56. Thompson et al. also reported that ferrite with 19.5% pearlite has a relative permeability of 280 whilst Jiles et al. [17] reported the permeability in a very low-carbon steel (0.0065 wt% C) as being 350 ± 50. It should be noted that the relative permeability values are also affected by factors such as ferrite grain size, pearlite interlamellar spacing, texture, stress and temperature [16,18]. In this work room temperature measurements on stress free samples (no applied stress and in a hot rolled or heat treated condition) have been made. In terms of microstructural parameters, the variation in phase balance has the dominant effect on the relative permeability values and is considered in this work.

4. FEM simulation

The 2D FE microstructure model used in this study is similar to that used by Hao et al. with conditions that the top and bottom boundaries of the sample were set with a magnetic potential of 1 and 0, respectively, to generate a uniform horizontal magnetic field. The left and right boundaries of the sample were set as electric insulation (magnetic field normal to the boundary) to eliminate the demagnetising field, this is termed "condition 2" as described in [8]. Greyscale optical micrographs of the ferrite/pearlite microstructures with different ferrite fractions were converted to black and white binary images and imported into the COMSOL model. In this modelling work the relative permeability of pearlite and ferrite are set as 58.6 and 330 respectively. The relative permeability of the mixture was calculated using parameters derived within the COMSOL software:

$$\mu_e = \frac{B_{ave}}{\mu_0 H_{ave}} \tag{2}$$

where B_{ave} is the average flux density inside the sample, μ_0 is the permeability of free space, and H_{ave} is the average magnetic field inside the sample.

The FE modelled results of the relative permeability change with ferrite fraction compared with the power law models and the experimentally fitted results are shown in Fig. 4. It can be seen that the FE modelled permeability value gives best fitting with the experimental data. The power law models with reported β values of 1/2 and 1/3 give higher relative permeability values than the experimental measured ones. In order to get a close fitting, a β value of 1/5 has been found to fit well with the measured values except for the low ferrite fraction (9%) sample. This β value has not been reported in the literature. It is apparent that the effect of low ferrite volume fractions on the relative permeability values for ferrite–pearlite is more significant than previously reported results for ferrite–austenite phase balance [8]. This is because pearlite is a ferromagnetic phase at room temperature, therefore when the ferrite fraction is low (ferrite grains are isolated), the magnetic flux can more readily pass through pearlitic regions between the preferred ferrite regions, whereas the austenite phase is less favourable hence a more complex route between ferrite regions, to minimise passage in austenite, occurs (shown in Fig. 5). Therefore, the previous results for the shape of the permeability-ferrite fraction relationship in ferrite–austenite cannot be simply applied, as this will give errors in predicting relative permeability values for low ferrite fractions in ferrite–pearlite microstructures (and hence any dual phase steels where the second phase is ferromagnetic).

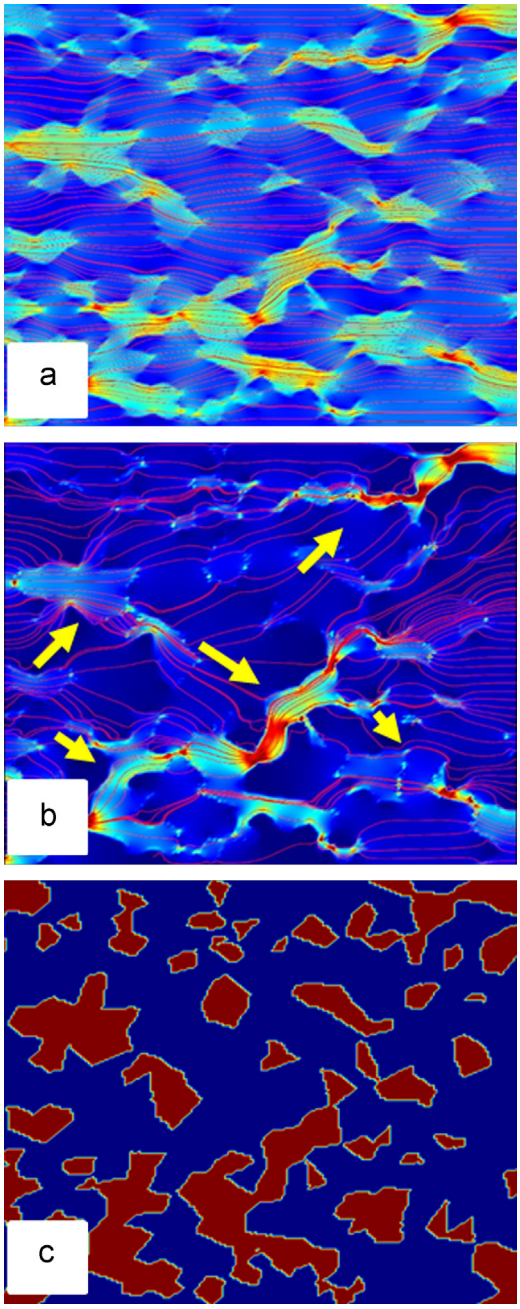

Fig. 5. FE Modelled results of magnetic flux distribution with the 30% ferrite in (a) ferrite–pearlite and (b) ferrite–austenite phase balance. (Stream line: magnetic flux density, arrows showing clear deviation to the ferrite in ferrite–austenite mix); (c) processed micrograph showing phase distribution of ferrite (red) and pearlite/austenite (blue). (For interpretation of the references to colour in this figure legend, the reader is referred to the web version of this article.)

Using the approach described above, it is possible to predict the effective permeability of any dual phase (or indeed multi-phase) microstructure provided that each single-phase relative permeability values are known, whereas power law models cannot easily deal with triple phase microstructures. The relative permeability values of other single phase steel microstructures (bainite and martensite) will

be reported separately, along with details of the relative permeability dependence on factors such as grain size, pearlite interlamellae spacing and bainite/martensite lath spacing etc [19–21].

5. Conclusions

In conclusion, a multi-frequency EM sensor has been used to measure the microstructure in ferrite+pearlite steels with different carbon contents. With an increase in pearlite content (up to 90%), the relative permeability and hence inductance value decreases. A 2D COMSOL FE model including microstructure has been shown to match the experimental results, therefore indicating that the technique can be used to non-destructively measure the ferrite fraction (up to approximately 90% ferrite) in ferrite/pearlite, or other dual phase, microstructures. The study shows that it may be possible to measure the phase fraction of ferrite of any dual phase steels using an EM sensor.

Acknowledgement

The authors thank the United Kingdom Engineering and Physical Sciences Research Council (EPSRC Grant reference: EP/H023429/1) and Tata Steel for their support of this research.

References

[1] Bhadeshia HKDH, Honeycombe SR. Steels - Microstructure and Properties. 3rd ed.. Oxford: Butterworth-Heinemann; 2006.
[2] Chatterjee S, Verma AK, Sharma V. Scr Mater 2008;58:191–4.
[3] Kitagawa H, Sohmura T. Trans ISIJ 1985;23:543–9.
[4] Gaujé P. Rev Met CIT 1990:1145–50.
[5] Astill AG, Tweed JH, Stacey K, Moss BC. Proc IoM Conf, Lond 1999:27–8.
[6] Papaelias M, Strangwood M, Peyton A, Davis C. Metall Mater Trans A 2004;35:965–72.
[7] Yin W, Hao X, Peyton A, Strangwood M, Davis C. NDT E Int 2009;42:64–8.
[8] Hao XJ, Yin W, Strangwood M, Peyton AJ, Morris PF, Davis CL. NDT E Int 2010;43:305–15.
[9] Hao XJ, Yin W, Strangwood M, Peyton AJ, Morris PF, Davis CL. Scr Mater 2008;58:1033–6.
[10] Hao XJ, Yin W, Strangwood M, Peyton AJ, Morris PF, Davis CL. Metall Mater Trans A 2009;40:745–56.
[11] Yin W, Peyton AJ, Strangwood M, Davis CL. J Mater Sci 2007;42:6854–61.
[12] Looyenga H. Physica 1965;31:401–6.
[13] Birchak JR, Gardner LG, Hipp JW, Victor JM. Proc EEEEE 1974;62:93–8.
[14] Davis CL, Dickinson SJ, Peyton AJ. Ironmak Steelmak 2005;32:381–4.
[15] Liu J, Hao XJ, Zhou L, Strangwood M, Davis CL, Peyton AJ. Scr Mater 2012;66:367–70.
[16] Thompson SM, Tanner BK. J Magn Magn Mater 1993;123:283–98.
[17] Jiles DC. J Phys D: Appl Phys 1988;21:1186.
[18] Cullity BD, Graham CD. Introduction to Magnetic Materials. 2nd edition, 2008.
[19] Zhou L, Liu J, Hao X, Strangwood M, Davis C. Int Conf NDE Steel, Jamshedpur, India 2011:208–15.
[20] Balamurugan S, Bhattacharyya T, Gudhae D, Zhou L, Davis CL, Peyton AJ, et al. Insight – Non-Destr Testing Cond Monit 2013;55:132–5.
[21] Zhou L, Strangwood M, Davis CL, Peyton AJ, Parker SV, Smith AWF, et al. Proceedings of the 9th International Rolling Conference 2013.